Replicating Mars' Climate: Applying a One-Dimensional Energy Balance Climate Model

Rebecca J. Hedley
Level 4 Project, MPhys Physics
Supervisor: Drs. Richard Wilman and Craig Testrow
Department of Physics, Durham University

Submitted: January 8, 2024

Mars presents a complex case study of climate change given its history as a periodically warm and wet planet, with applications to astrobiology and understanding greenhouse feedback mechanisms on Earth. A one-dimensional energy balance model (EBM) is built using the finite difference method, based on a differential equation encompassing the effects of heat capacity, solar insolation, albedo, meridional heat diffusion, and outgoing radiation. Mean annual temperature values agree to a latitudinally averaged value of 1% to Earth climate fit from literature, and to within 3.2% when the same model is applied to Mars. Seasonal variations are clearly observed in the model and replicate more extreme variations expected on Mars, as well as the combined effects of obliquity and an eccentric orbit. Further work involving CO_2 cycle modelling is discussed to improve the Mars model given the importance of the annual pressure cycle.

CONTENTS

I. Introduction 2
A. Motivation 2
B. Climate Modelling 3
1. Energy Balance Models 3
2. General Circulation Models 3

II. Theory and Methods 3
A. Energy Budget 3
1. Incoming Flux 4
2. Outgoing Flux 4
B. One-Dimensional EBM 5
C. Model solving 6

III. Results and Discussion 6

IV. Further Application to Mars 9
A. Carbon Dioxide Cycle Modelling 9

References 10

I. INTRODUCTION

A. Motivation

Mars' current climate is cold and dry, and its atmospheric volume is less than 1% of Earths. No climate model predicts ancient Martian temperatures breaking freezing temperatures. Despite this, there exists evidence for an active hydrological cycle in its past. As a result of its absence of plate tectonics, an ecosystem, or global oceans, the Martian surface is preserved well enough for study of eras as early as the Noachian (3.5 - 4.1Ga). Branching tributaries beginning near geographic peaks indicate precipitation, and the large valley networks these create are expected to have formed over timescales of 10^5 - 10^7 years, indicating a consistently active water cycle [13]. Though it seems uncommon, anomalous landforms most apparent near the poles point towards some glaciation as a result of both meltwater and movement of ice sheets - as early as the Noachian period and possibly as late as the early Amazonian (0 - 3.0Ga) [14]. Surface temperatures would need to increase by 25-50K from modern values to accommodate meltwater glaciation, again pointing towards a warmer climate.

It is unlikely that Ancient Mars' wet climate was similar to that of Earths. Constraints on luminosity, orbit, and radiative transfer disfavour a warmer climate soley as a result of CO_2, suggesting that the water cycle was limited in volume and intermittent during the ancient Noachian period. Geophysical evidence supports this, given that the lack of consistent glaciation similarly points towards a small water inventory [22]. The geochemistry of Mars also suggests a mostly dry surface: aluminium-rich clays, and aqueous minerals like chlorides, silicas, and sulphates (which require water to form) are abundant in Noachian geology, yet carbonates, which form readily on warm and wet surfaces, are almost absent [20] [21]. Seemingly contradictory evidence makes it clear that Mars has a complex history. Still, the warming mechanism to allow episodic warm and wet periods is unclear. The possibility of modelling a CO_2 driven greenhouse effect on Mars is discussed later in section **IV.A**.

With climate studies, we can make preliminary insights into whether Mars could have, or can in the future, host life. Appropriate conditions for liquid water are widely used as the basic criteria for a habitable planet, and while temperature conditions up to boiling point may seem too broad, extremophiles are capable of existing under such conditions. Microorganisms isolated on Earth have displayed the ability to thrive at low temperatures, and even in simulated Martian environments: *H. hispanica* and *G. thermantarcticus* are just two extremophiles that resisted days of Martian temperatures and pressures in lab conditions [16]. One-dimensional EBMs are therefore important to be able to assess temperatures at various latitudes and points in orbit - by the seemingly broad liquid water definition of habitability, even the Earth is only partially habitable.

Additionally, the study of Mars' climate allows insight into climate change mechanisms. It's clear that human activity is capable of globally changing the environment, and it is strongly suggested that action is taken to prevent any further warming [15]. The process of developing accurate climate models aids this purpose, in addition to exploring the efficiency of warming and cooling mechanisms for application to the Earth.

B. Climate Modelling

1. Energy Balance Models

Energy balance models predict global temperatures by a radiative energy budget, estimating energy received from the Sun and energy retained or reflected by the planet. The most simple EBM is the zero-dimensional case, a model which predicts a single mean surface temperature to the whole planet by assuming that the energy received is equal to the energy lost in a steady state solution. The 0D EBM neglects varying land distributions (and therefore temperature-dependent heat capacities, albedo values, and outgoing radiation) and heat diffusion between latitudes. They can provide relatively accurate estimates for global mean temperature [12], however they cannot provide temperature as a function of latitude, and so are not appropriate for this study of Mars' climate.

One-dimensional EBMs, such as the model used in this study, split the planet into latitude bands and assess the temperature of each based on local variables such as solar insolation and ice distribution. 1D EBMs most importantly allow for meridional heat transport, an important factor in the local latitudinal energy budget for planets with a thick enough atmosphere [1], and therefore important for the Earth validation study and later, a study of Mars' pressure variations. As a result of the inclusion of heat diffusion, it is possible that each region at any particular time will not locally satisfy the energy budget condition Eq. 1. This is also possible for the planet as a whole on any day, especially due to an eccentric orbit.

2. General Circulation Models

General circulation models (GCMs) are more complex three- (or four-) dimensional climate models which are based on fluid equations. Earth is split into horizontal grid cells longitudinally and latitudinally, and also split vertically based on height from surface or pressure. Systems which apply on scales smaller than that of the resolution of the grid, such as ice-albedo feedback or cloud effects on radiative flux, are parametrised, and these parametrisations create the largest source of error within a GCM [10]. Despite this, GCMs remain the most accurate computational representations of climate.

GCMs have had success modelling the $\mathrm{CO_2}$ cycle on Mars. Unlike EBMs, which assume $\mathrm{CO_2}$ condenses directly on the surface, GCMs allow for $\mathrm{CO_2}$ condensing in the atmosphere. Atmospheric $\mathrm{CO_2}$ behaves much differently to ice cap $\mathrm{CO_2}$ in that, whereas ice deposits are effectively transparent at infrared wavelengths, atmospheric $\mathrm{CO_2}$ particles efficiently scatter heat and therefore contribute to global cooling. Such effects on Mars have been observed to decrease total polar condensation rates by 10 - 20% during the winter [11], therefore also affecting ice-albedo feedback and decreasing heat diffusion due to a reduced atmosphere.

II. THEORY AND METHODS

A. Energy Budget

EBMs assume that atmospheric temperature is assessed by equilibrium between energy sources and losses. The infrared radiation $I(T)$ received and retained by the atmosphere is dependent on the total solar flux S received annually, and the global planetary albedo A ,

$$I(T) = S(1 - A(T)). \tag{1}$$

1. Incoming Flux

Total solar flux in each latitude band is proportional to the cosine of solar zenith angle z, which is expressed as a function of latitude θ, solar hour angle h, and solar declination δ:

$$\cos z = \sin\theta \sin\delta + \cos\theta \cos\delta \cos h. \tag{2}$$

The declination angle is a sinusoidal function dependent on orbital longitude and obliquity δ_0, which reaches its extrema at the solstices. Solar hour angle describes the angular displacement of the Sun in a planets sky from the meridian, and is zero degrees at noon. In order to find a diurnally averaged value for incoming solar flux, the cosine of solar zenith angle z must be averaged over one rotation. First it is averaged over solar hour angle h = - H to + H, with H as radian half-day length,

$$H = \arccos(-\tan\theta \tan\delta), \tag{3}$$

which corresponds to the fraction of a day during which the sun is above the horizon.

$$\overline{\cos z} = \frac{\int_{-H}^{H} \sin\theta \sin\delta + \cos\theta \cos\delta \cosh dh}{\int_{-H}^{H} dh} = \sin\theta \sin\delta + \cos\theta \cos\delta \frac{\sin H}{H}. \tag{4}$$

If, during summers at the poles for example, the sun remains above the horizon for a complete day then $H = \pi$ according to the above definition. At latitudes where the Sun remains in the sky for a fraction of a rotation, the average $\overline{\cos z}$ must be scaled then by $\frac{H}{\pi}$. In order to generalise to any planet with semimajor axis a in AU, Eq. 4 is also scaled by a $\frac{1}{a^2}$ term. Multiplying by these factors and also by solar constant q, we find diurnally averaged incident solar flux S_0,

$$S_0 = \frac{q}{\pi}\left(\frac{1.0AU}{a}\right)^2 (H \sin\theta \sin\delta + \cos\theta \cos\delta \sin H). \tag{5}$$

As of yet, we have assumed a circular orbit. Total insolation received by a planet at a given time is a function of the position in its orbit (given that the orbit is not perfectly circular), and the solar zenith angle at each latitude. The instantaneous Sun-planet distance is given by the following expression,

$$r = \frac{a(1-e^2)}{1 + e\cos\theta} \tag{6}$$

where e is the eccentricity of the orbit, a is its semimajor axis, and θ is the true anomaly, an angular quantity which defines the position of a body in its orbit in respect to its periapsis. From the instantaneous position r we can then include the effect of eccentricity on daily insolation by invoking the inverse square law,

$$S_{eccentric} = \frac{S_0}{r^2}, \tag{7}$$

where S_0 is the original expression Eq. 5 derived for a body with zero orbital eccentricity.

2. Outgoing Flux

Three prescriptions were tested for infrared cooling and albedo functions. The first two assume that the planet is a blackbody and therefore radiates energy proportional to T^4, which

Model	IR Cooling Function	Albedo Function
1	$I(T) = \frac{\sigma T^4}{1+\frac{3}{4}\tau_{IR}^0}$	$A(T) = 0.5 - 0.2\tanh\frac{T-268}{5}$
2	$I(T) = \frac{\sigma T^4}{1+\frac{3}{4}\tau_{IR}(T)}$	$A(T) = 0.525 - 0.245\tanh\frac{T-268}{5}$
3	$I(T) = A + BT$	$A(T) = 0.475 - 0.225\tanh\frac{T-268}{5}$

TABLE I: Model 1 has fixed optical thickness τ_{IR}^0 = 1. Model 2 has temperature dependent optical thickness $\tau_{IR}(T) = 0.79(T/273)^3$. Model 3 has constants A = 2.033 $\times 10^2 Jm^{-2}s^{-1}$, B = 2.094 $Jm^{-2}s^{-1}K^{-1}$

.

is then reduced through an optically thick atmosphere which reradiates heat back to the planet. The two models differ in that the second has a temperature dependent optical thickness, $\tau_{IR}(T)$, which acts to decrease infrared radiation escaping the atmosphere as the surface temperature increases. This reflects the temperature-dependent greenhouse effect, in which heat retention scales with the amount of water vapour in the atmosphere due to absorption. The third model is a simple linear relation obtained by applying a least squares fit to outgoing infrared flux data from satellite observations. The τ_{IR} models are borrowed from SMS08 [1], and the linear model is borrowed from NC79 [4]. These are outlined in Table I.

Albedo is dependent on fractional ice and snow cover, so varies according to temperature. In each formulation, surface albedo is parametrised to be between 0.25-0.3 for ice-free surfaces above 273K, and 0.7-0.77 for ice-covered surfaces below 263K, in line with observational data [5] [6]. The albedo function is adapted to transition between ice-free and ice-covered at the freezing point of CO_2 when the model is applied to Mars. The hyperbolic tangent form ensures a smooth transition between ice-covered and ice-free states.

B. One-Dimensional EBM

The one-dimensional model concerns heat diffusion, solar insolation, and outgoing infrared radiation, represented by the following differential equation,

$$C\frac{\partial T}{\partial t} = S(1-A) + \frac{\partial}{\partial x}[D(1-x^2)\frac{\partial T}{\partial x}] - I, \tag{8}$$

where C is heat capacity, S is the daily averaged solar insolation, A is the albedo, D is the diffusion coefficient, and $x \equiv \sin\lambda$ is the sine of the latitude. It is possible, by a change of variable from x to λ, to express this in terms of latitude,

$$C\frac{\partial T}{\partial t} = S(1-A) + D\frac{\partial^2 T}{\partial t^2} - D\tan\lambda\frac{\partial T}{\partial \lambda} - I, \tag{9}$$

which is the expression used in the final computational model. Each of these values, except D, is local to its latitude band.

The value of heat capacity is determined by the distribution of land, ocean, and ice (each with a different value of C). Uniform land/ocean distribution (30% land, 70% ocean) is assumed in every latitude band, and the proportion of ocean which is covered by ice is determined by the temperature at that band - bands below 263K are completely ice-covered, bands between 263-273K are partially ice-covered, smoothly increasing oceanic ice fraction f_{ice},

$$f_{ice} = 1 - e^{\frac{T-273}{10}}, \tag{10}$$

as the temperature drops, and bands above 273K are ice-free. Prescribed heat capacities are as follows: C_{land} = 5.25 $\times 10^6$ $\mathrm{Jm^{-2}K^{-1}}$, C_{ocean} = 40 C_{land}, C_{ice} = 9.2C_{land} when 263K $< T <$ 273K, and C_{ice} = 2.0C_{land} when $T \leq$ 263K. This is what makes the snowball transition almost impossible to transition out of - retained heat is reduced to approximately 30% of the incoming value by a large albedo, and a larger heat capacity for ice, meaning melting ice requires heat transport from warmer latitudes. This is not viable on an ice-covered planet. As discussed above, S varies latitude to latitude given its dependence on the solar zenith angle, and A similarly depends on the land, ocean, and ice distribution.

D is a function of atmospheric pressure p, atmospheric heat capacity c_p, rotation rate Ω, and mean molecular weight of the atmosphere m. D_0 denotes the diffusion coefficient value for Earth, taken to be 5.394 $\times 10^{-1}$ $\mathrm{Jm^{-2}s^{-1}K^{-1}}$, and similarly for other values the subscript 0 denotes the Earth value - p_0 = 1 atm by definition, c_{p_0} = 1000 $\mathrm{g^{-1}K^{-1}}$, m_0 = 28, and Ω_0 = 7.27 $\mathrm{rads^{-1}}$.

$$\frac{D}{D_0} = \frac{p}{p_0}\frac{c_p}{c_{p_0}}\frac{{m_0}^2}{m}\frac{{\Omega_0}^2}{\Omega} \tag{11}$$

For the Earth validation model, D is a constant since we don't consider pressure variations. Such variations will become important when modelling Mars' climate given the severe seasonal CO_2 pressure changes of around 30% annually [8].

C. Model solving

The above differential equation, Eq. 9, is solved using the finite difference method. The planet is split into 32 latitude bands corresponding to a separation of $\sim$5.6°, as this chosen value demonstrates the best numerical stability. The climate evolves with a time-step δt = 1 day; given that the solar irradiation is averaged over one day this time-step should not be smaller than one day.

The model is initialised as an isothermal planet above freezing point (300K), at the winter solstice. Initialising well above freezing significantly reduces the chance of a snowball transition to an ice-covered planet. Stability of the model was tested by artificially injecting extreme temperatures (i.e. 0K bands) once the model had settled. This was performed at various latitudes and the model recovered from all temperature injections within 2 orbits.

III. RESULTS AND DISCUSSION

The model is initially ran under Earth parameters, and compared to an observational fit, to validate the accuracy of the model and to assess its convergence. Further, the model is applied to Mars. Results for dirunally averaged incident solar flux on Earth are compared to the average daily flux at top-of-atmosphere for 2023 as tabulated in [19]. Model flux matches the tabulated data to within 0.1%, and is shown in Fig. 1.

The model solution under Earth parameters is compared to an empirical model formulated from observational data [4],

$$T(x) = 302.3 - 45.3\sin^2\lambda, \tag{12}$$

where $x \equiv \sin\lambda$. This fit does not account for asymmetric seasonal variations induced by the inclusion of Earths obliquity, regardless, it describes the planets annual mean temperature per latitude well enough to assess the models' validity. A ten-year running annual mean is taken after every year of the models evolution past year 9. The mean relative difference across all

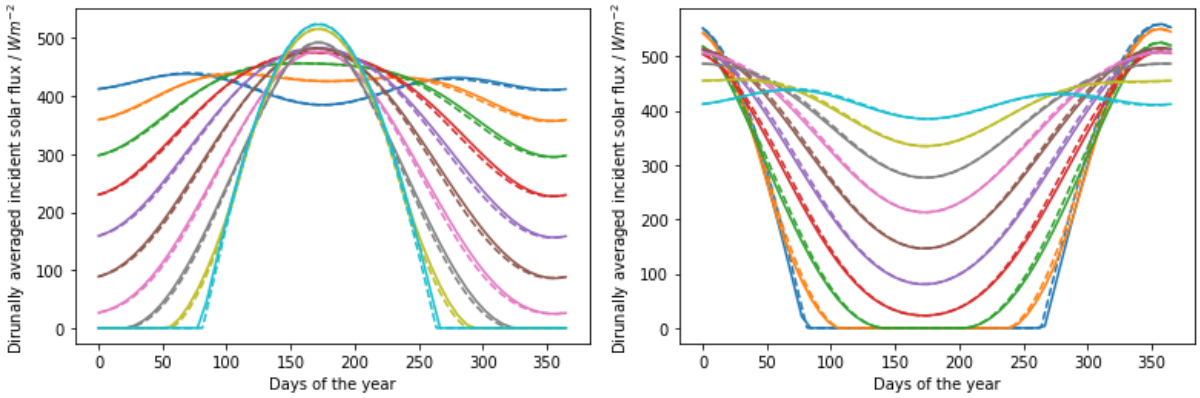

(a) Northern hemisphere **(b)** Southern hemisphere

FIG. 1: Model data (dashed line) plotted against tabulated data (solid line) for Earths a) Northern, and b) Southern hemispheres.

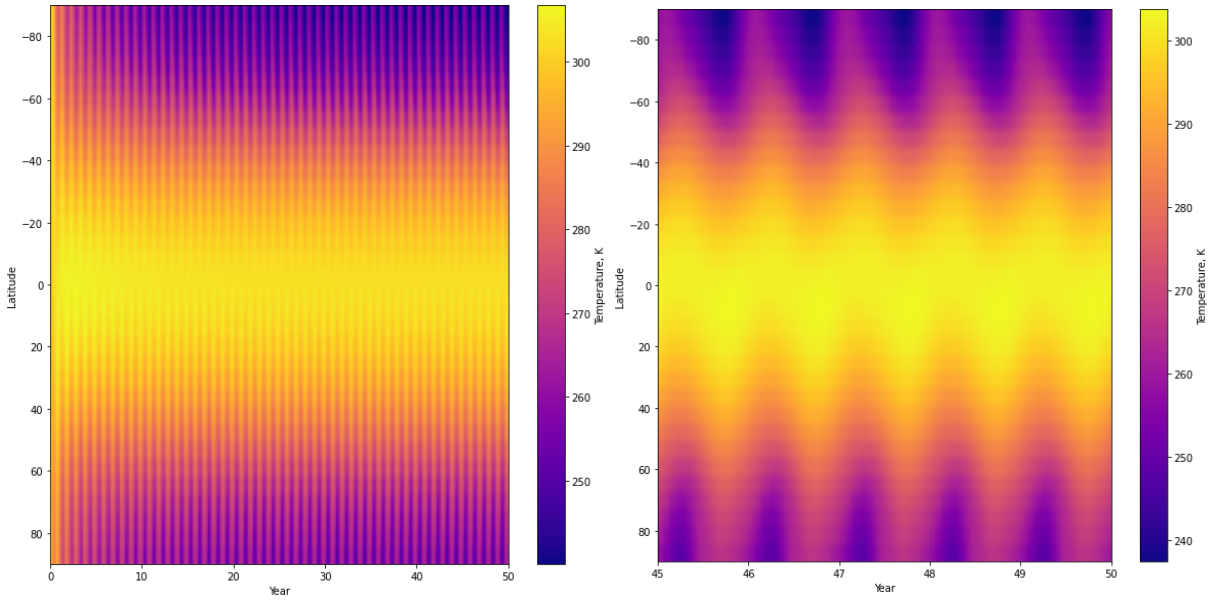

(a) Heatmap of Earth climate between 0 - 50 years **(b)** Heatmap of Earth climate last 5 years of modelling

FIG. 2: Heatmaps displaying Earth's climate (Kelvin) 50 years post model initialisation. Full heatmap (a) displays temperatures plotted every 73 days, settled heatmap (b) shows temperatures plotted every 5 days. Negative latitudes (degrees) correspond to the Southern hemisphere.

latitudes is taken. The Earth model settles to a less than 1% difference to the empirical model. Convergence is assessed by comparison to the above fit (Eq. 12) every year, and also comparison to the models own temperatures at the same point in orbit each year. The convergence tests are found in Fig. 3.

Mars' model climate is compared to an analytical fit [7] which is based on results from the NASA Ames GCM for a 7 millibar atmosphere,

$$T(x) = \frac{q_0}{4\sqrt{1-e^2}}\frac{S_{a_0}}{B} - \frac{A}{B} + \frac{q_0}{4\sqrt{1-e^2}}\left(\frac{S_{a_2}p_2(x)}{6D+B} + \frac{S_{a_4}p_4(x)}{20D+B}\right), \tag{13}$$

where q_0 is the solar constant at Mars, e is eccentricity, D is diffusivity, and $x \equiv \sin\lambda$ is the sine of the latitude. A, B, and S_{a_n} are adjustable fitting parameters and p_n are the Legendre

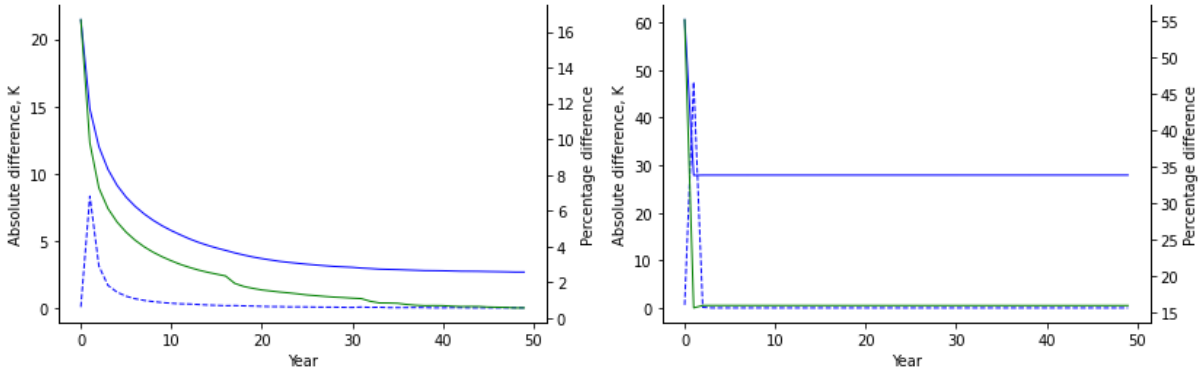

(a) Earth convergence tests **(b)** Mars convergence tests

FIG. 3: Convergence tests for both planet models. Blue tests indicate comparison to empirical models Eqs. 12, 13 by absolute (solid line) and percentage (dashed line) difference. Green test shows change in temperature compared to same time last year, $\delta = |T_{year} - T_{year-1}|$. The average difference is taken at the Southern summer solstice.

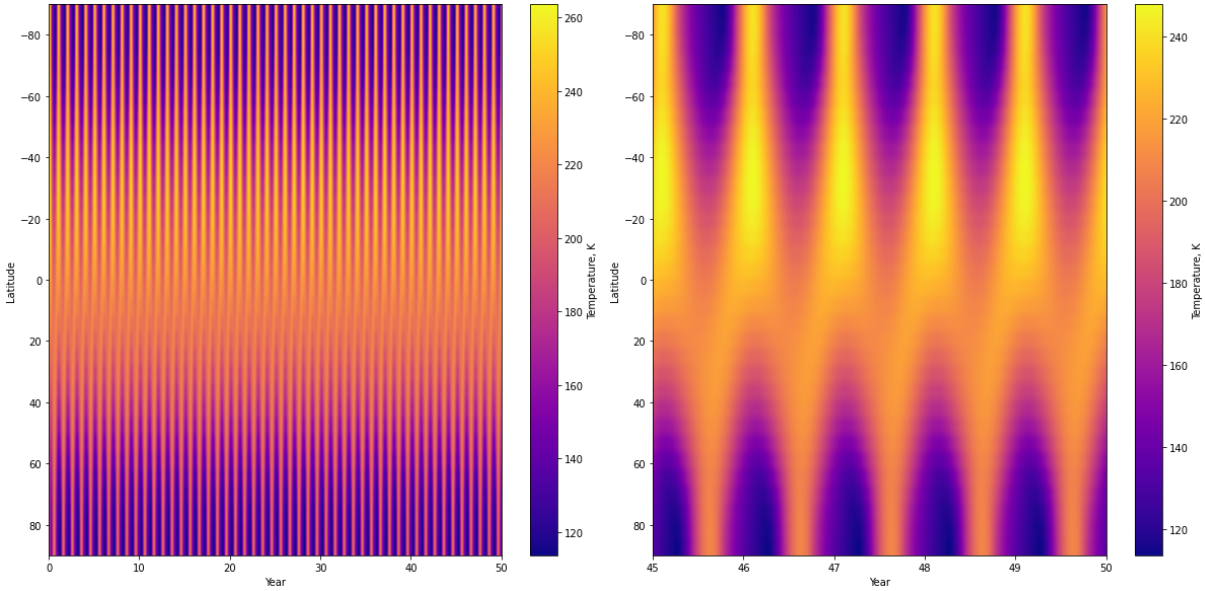

(a) Heatmap of Mars climate between 0 - 50 years **(b)** Heatmap of Mars climate last 5 years of modelling

FIG. 4: Heatmaps displaying Mars' climate (Kelvin) 50 years post model initialisation. Full heatmap (a) displays temperatures plotted every 3 days, as does settled heatmap (b). Negative latitudes (degrees) correspond to the Southern hemisphere.

polynomials.

The model settles to a 16% difference averaged over all latitudes to the model, although it is noted that this is taken as a latitudinal average on one day during the Southern summer and compared to annually averaged fit Eq. 13. Mean difference between the ten-year average and the analytical fit is 4.2K or 3.2%. Mars' heatmap displays much more relatively extreme summers and winters than Earth, as expected due to a much sparser atmosphere allowing for little heat diffusion (which is reflected in the diffusivity coefficient D for each planet). The Southern hemisphere displays characteristically hot summers and cold winters relative to the milder North. The assumption of equal land:ocean distribution in each latitude band is more

justified in the case of Mars than Earth considering it is 100% land.

The latitude separation is chosen to be the smallest latitude separation which provides a numerically stable solution. A smaller latitude separation introduces oscillations at the boundaries (poles), known as Runge's phenomenon, which occasionally propagate. The oscillations are mitigated by taking a ten-year mean which converges as expected without any repercussions from the oscillations. Runge's phenomenon can further be mitigated by using a set of nodes which are denser near the boundaries. Nonetheless, the Earth models convergence to within 1% of the observational fit indicates that the solution is well-resolved enough to represent the climate.

The model settles to the same solution regardless of the season it is initialised in, however, it is sensitive to initial temperature. Initialised above freezing point, the Earth model settles to a climate representative of modern Earth, but at freezing point (273K) or below it settles to an ice-covered solution. Mars settles to the temperature distribution displayed in Fig. 4. regardless of the initial temperature being above or below freezing point. The inclusion of a warming mechanism, like $\mathrm{CO_2}$, is necessary for exploration of the possibilities of warm ancient Mars.

The three infrared radiative functions largely behave the same, though function 2 was chosen for its temperature-dependent optical thickness which describes the attenuation of radiation by Earths atmosphere. This is likely not an accurate representation of outgoing radiation on a planet, such as Mars, with a dry 7 millibar atmosphere. With an outgoing radiation function reflective of Mars' atmosphere, the solution would likely be cooler than the model currently settles to. Further, it will be important to alter the outgoing infrared radiation as a function of $\mathrm{CO_2}$ content in the atmosphere in order to simulate the greenhouse effect on a Mars that possibly had a much higher $\mathrm{CO_2}$ partial pressure than today.

IV. FURTHER APPLICATION TO MARS

A. Carbon Dioxide Cycle Modelling

It is assumed that the amount of $\mathrm{CO_2}$ adsorbed and released from the regolith annually is negligible, so that the total conserved amount of $\mathrm{CO_2}$ on Mars is always split between ice on the ground and gaseous $\mathrm{CO_2}$ in the atmosphere. Previous EBMs have also excluded the contribution of the regolith and reached the same conclusions as models including it [9]. It is also assumed that the entire atmosphere is composed of $\mathrm{CO_2}$ (reasonable given that it is in reality 95.32% $\mathrm{CO_2}$ [17]). To include the effects of $\mathrm{CO_2}$ condensation and sublimation on temperature, a latent heat term is required to alter Eq. 9.,

$$C\frac{\partial T}{\partial t} = S(1-A) + \frac{\partial}{\partial x}[D(1-x^2)\frac{\partial T}{\partial x}] - I + LM, \tag{14}$$

where L is the latent heat per unit mass of $\mathrm{CO_2}$, and M is the mass of $\mathrm{CO_2}$ which condenses or sublimates per unit time. Sublimated $\mathrm{CO_2}$ contributes to the atmospheric pressure, which affects the diffusion coefficient D as described in Eq. 11. Mass M condensed is a function of frost point temperature T_c, which is itself a function of pressure p,

$$T_c = \frac{3148.42}{26.388 - \ln p}, \tag{15}$$

where p is measured in $\mathrm{kgm^{-2}}$ [23]. Condensation of $\mathrm{CO_2}$ releases latent heat, which warms the local atmosphere, and as a result atmospheric temperature never drops below freezing point.

Conversely, energy added to the system sublimes frozen CO_2, and heats the atmosphere once the surface is ice-free. If all of the CO_2 were to condense, thus allowing temperature to drop, the atmosphere would have collapsed in which case the model would not apply (the solar flux received by Mars would not allow the temperature to drop this low regardless).

The atmosphere-ice CO_2 split is determined by conservation of mass,

$$M_{total} = M_{atmosphere} + M_{ice}, \tag{16}$$

where the mass of condensed CO_2 is determined by the areal extent of the polar ice caps. In turn, mass of CO_2 in the atmosphere is determined by assuming a conserved total CO_2 mass M_{total}.

Rather than reusing the outgoing radiation prescriptions proposed in section **II. A.**, the partial pressure of CO_2 should be considered in a parametrisation of outgoing IR. *Nakamura and Tajika* achieved this with a linear function of the same form as model 3 in table I, where coefficients A and B were simple functions of the surface pressure of CO_2 above and below freezing point [9]. This would allow the inclusion of the greenhouse effect which is integral to finding a warm and wet model solution on Mars.

The addition of the CO_2 cycle can improve the representation of Mars' modern climate, as discussed, however it also allows insight into the ancient Martian climate. Carbon sinks such as deep carbonates, and CO_2 losses from the late heavy bombardment are estimated to have resulted in the loss of several bars of CO_2 from Mars, which could have been a major contributor to the greenhouse effect [18]. Exploring the possibility of a thick CO_2 atmosphere requires the inclusion of a latent heat term. While CO_2 remains a major factor in warming early Mars, it still seems an impossibility with CO_2 as the sole mechanism, and it is likely a combination of greenhouse gases that resulted in Mars' periodically warm climate [13].

REFERENCES

[1] D. Spiegel, K. Menou, C. Scharf., "Habitable Climates", The American Astronomical Society, vol. 681, 1609-1623 (2008).

[2] D. Williams, J. Kasting., "Habitable Planets with High Obliquities", Icarus, vol. 129, 254-267 (1997).

[3] J. Appelbaum, D. J. Flood., "Solar Radiation on Mars", Lewis Research Center, Cleveland, Ohio, Tech. Memorandum 102299, 1989.

[4] G. R. North, J. A. Coakley., "Differences between Seasonal and Mean Annual Energy Balance Model Calculations of Climate and Climate Sensitivity", Journal of the Atmospheric Sciences, vol. 36, 1189-1204 (1979).

[5] P. R. Goode et al., "Earthshine Observations of the Earth's Reflectance", Geophysical Research Letters, vol. 28, 1671-1674 (2001).

[6] D. K. Perovich, C. Polashenki., "Albedo evolution of seasonal Arctic sea ice", Geophysical Research Letters, vol. 39 (2012).

[7] A. Kling, R. Haberle., "An analytical climate model to reproduce first order, yearly-averaged, climatology on early Mars: implications for the ancient lakes in the Gale crater", European Planetary Science Congress, vol. 12, 697 (2018).

[8] F. Forget, F. Hourdin, O. Talagrand., "CO_2 Snowfall on Mars: Simulation with a General Circulation Model", Icarus, vol. 131, 302-316 (1998).

[9] T. Nakamura, E. Tajika., "Stability and evolution of the climate system of Mars", Earth Planets Space, vol. 53, 851-859 (2001).

[10] P. Ceppi et al., "Cloud feedback mechanisms and their representation in global climate models", Wiley Interdisciplinary Reviews.

[11] F. Forget, J. B. Pollack., "Thermal infrared observations of the condensing Martian polar caps: CO_2 ice temperatures and radiative budget", Journal of Geophysical Research, vol. 101, 16865-16880 (1996).

[12] G. Lohmann, "Temperatures from energy balance models: the effective heat capacity matters", European Geosciences Union, vol. 11, 1195-1208 (2020).

[13] R. D. Wordsworth, "The Climate of Early Mars", Annual Review of Earth & Planetary Sciences, vol. 44, 1-31 (2016).

[14] J. S. Kargel, R. G. Strom., "Ancient glaciation on Mars", Geological Society of America, vol. 20, 3-7 (1992).

[15] IPCC, 2023. *Climate Change 2023: Synthesis Report,* [Core Writing Team, H. Lee and J. Romero]. IPCC, Geneva, Switzerland, 35-115.

[16] V. Mastascusa *et al.,* "Extremophiles Survival to Simulated Space Conditions: An Astrobiology Model Study", Origins of Life and Evolution of Biospheres, vol. 44, 231-237 (2014).

[17] P. B. James, G. R. North., "The Seasonal CO_2 Cycle on Mars: An Application of an Energy Balance Climate Model", Journal of Geophysical Research, vol. 87, 10271-10283 (1982).

[18] B. M. Jakosky, "The CO_2 inventory on Mars", Planetary and Space Science, vol. 175, 52-59 (2019).

[19] G. Kopp, "Daily solar flux as a function of latitude and time", Solar Energy, vol. 249, 250-254 (2023).

[20] J. Carter *et al,* "Hydrous minerals on mars as seen by the crism and omega imaging spectrometers: Updated global view", Journal of Geophysical Research, vol. 118, 831–858 (2013).

[21] B. L. Ehlmann, C. S. Edwards, "Mineralogy of the Martian surface", Annual Review of Earth and Planetary Sciences, vol. 42, 291-315 (2014).

[22] J. L. Fastook, J. W. Head, "Glaciation in the late noachian icy highlands: Ice accumulation, distribution, flow rates, basal melting, and top-down melting rates and patterns", Planetary and Space Science (2014).

[23] *Handbook of Chemistry and Physics*, 36th ed., Cleveland, Ohio, Chemical Rubber Publishing Co. 1954, 2239-2244.